Convention Special Issue – 2020

J. Indian Chem. Soc.,
Vol. 97, No. 12a, December 2020, pp. 2541-2552

Electronic coupling in heterobimetallic porphyrin dimers: A spectroscopic investigation†

Satabdi Roy≠, Sayantani Banerjee≠, Sarnali Sanfui and Sankar Prasad Rath*

Department of Chemistry, Indian Institute of Technology Kanpur, Kanpur-208 016, Urrar Pradesh, India

≠Equal contribution.

E-mail: sprath@iitk.ac.in

Manuscript received online 16 November 2020, revised and accepted 27 December 2020

We have reported here the synthesis, structure and spectroscopic properties of Co(II)-Fe(III) heterobimetallic ethane and ethene-bridged porphyrin dimers and investigated spin coupling between two paramagnetic metal centers that would possibly occur either through the bond or through space. X-Ray structures of one homobimetallic and one heterobimetallic complexes are reported here. UV-Vis spectrum of heterobimetallic complex is clearly distinguishable from its homobimetallic analogs: a split in the Soret band is distinctly visible for homobimetallic complex while a sharp band was observed for heterobimetallic complex. Both Fe(III) and Co(II) centers are paramagnetic and interactions between them have been scrutinized using variable temperature NMR (in solution) and magnetic studies (in the solid state). ^{1}H NMR spectra of the heterobimetallic complexes are distinctly different compared to their homobimetallic analogs.

Keywords: Diheme enzymes, MauG analog, heterobimetallic complex, spin coupling, structure elucidation, NMR for paramagnetic molecules.

Introduction

Multiheme proteins and enzymes are one of the most fascinating molecular machines designed by Nature[1–3]. The relative arrangement of the heme centers and interaction between them have been found to exhibit various functions in a widely distributed family. Indeed, the presence of more than one heme center is known to provide an effective vehicle for modulating various structure and properties needed for its function[4]. Modulation of such intermacrocyclic interactions is crucial in the design of molecular machines and advanced functional materials.

Diheme enzymes such as cytochrome c peroxidase (bCcP) and MauG are known to catalyze various chemical transformations in biology[2,3]. In the X-ray structure of the enzymes (Fig. 1)[2a], two heme centers are physically separated while a tryptophan residue has been located between them. However, despite a large physical separation between the two heme units, electrons are efficiently shared between them through the tryptophan residue which possibly acts as a bridge between them[2]. For structure-function correlations

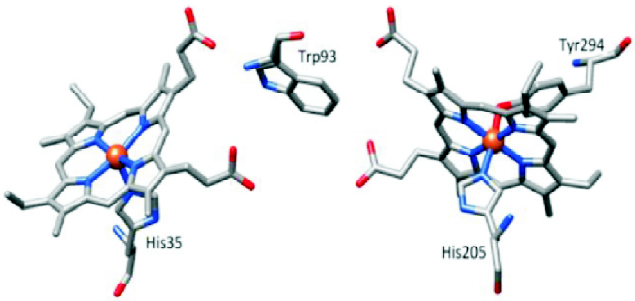

Fig. 1. Relative orientation of hemes and the intervening tryptophan residue in MauG (PDB ID code 3L4M)[2a].

of diheme proteins, covalently linked porphyrin dimers and their transition metal complexes have been investigated[4]. The nature of the spacer control the spatial arrangement and inter-macrocyclic interactions between them[4–14]. Our group has been actively involved working on synthetic dihemes in order to understand the Nature's design[4,8–13].

Heterobimetallic porphyrin dimers have attracted considerable attention as synthetic models of cytochrome c oxi-

†**Professor R. S. Varma Memorial Lecture (2020).**

dase, binding and activation of small molecules, electron transfers, catalysis, etc.[15]. In the present work, we have investigated ethane and ethene bridged cobalt(II)-iron(III) heterobimetallic porphyrin dimers and compared them with the corresponding homobimetallic dicobalt(II) and diiron(III) analogs reported earlier[12] by us. Spectroscopic investigations show evidences of electronic interaction between two metalloporphyrin centers.

Results and discussion

The free base ligand 1,2-bis(*meso*-octaethylporphyrinyl) ethane, (PD_1), was prepared using a procedure reported earlier[16]. To the chloroform solution of PD_1, one-equivalent $FeCl_2$ was added and refluxed for an hour under nitrogen atmosphere. The resulting solution was completely dried under vacuum and the mono-metallic complex, Fe(Cl)-PD_1, (Scheme 1) was isolated from the reaction mixture in pure form via column chromatography. Excess $Co(OAc)_2.4H_2O$ dissolved in methanol was then added to the chloroform solution of Fe(Cl)- PD_1 and the resulting mixture was refluxed under nitrogen atmosphere for an hour. The solution was evaporated to complete dryness and purified by column chromatography. The resulting heterobimetallic complex, CoFe(Cl)-PD_1 was characterized by UV-Vis-NIR, ^{1}H NMR and ESI-MS. Scheme 1 shows the synthetic outline for the formation of homo and heterobimetallic complexes. As compared to the UV-Vis spectrum of free base ligand (PD_1) (404 nm) in dichloromethane solution, a red shift in the Soret band (416 nm) of the UV-Vis spectrum occurs upon formation of the monometallated bisporphyrin, Fe(Cl)-PD_1, along with the appearance of a left shoulder (Fig. 2). Instead of the four Q bands in the free base, PD_1, three Q bands at 515, 553 and 576 nm appear in Fe(Cl)-PD_1. The UV-Vis spectrum of the heterobimetallic complex, CoFe(Cl)-PD_1 in dichloromethane displays a Soret band (405 nm) along with the appearance of two Q bands at 554 and 655 nm (Figs. 2 and 3).

Trans-1,2-bis(*meso*-octaethylporphyrinyl)ethene (PD_2) has been synthesized using a reported procedure[14]. The

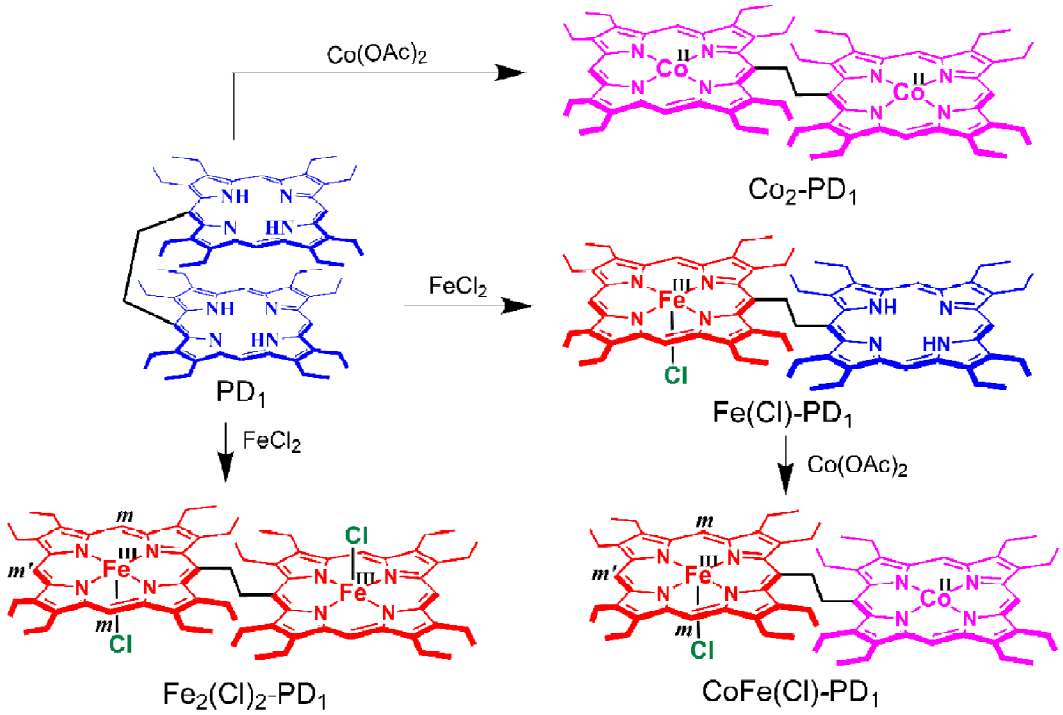

Scheme 1. Synthetic outline of the homo and heterobimetallic complexes using ethane-bridged porphyrin dimer. *Meso* positions (*m* and *m'*) are also assigned here.

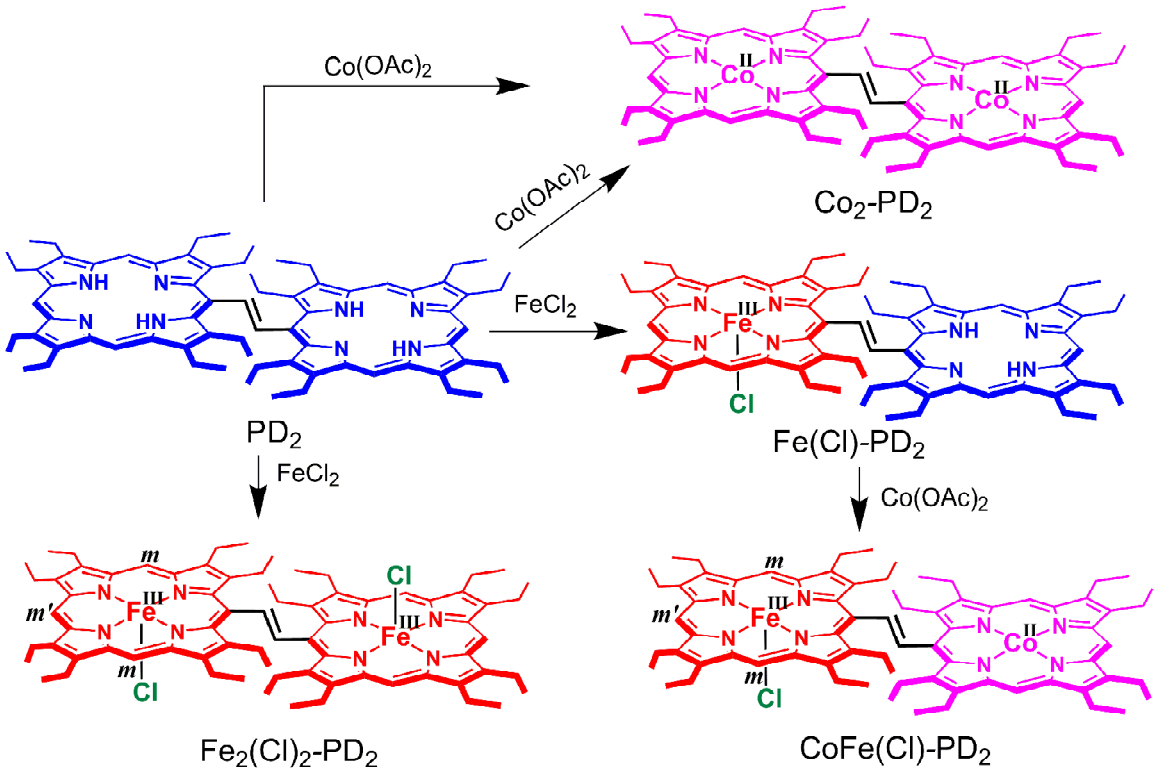

Scheme 2. Synthetic outline of the homo and heterobimetallic complexes using ethene-bridged porphyrin dimer. *Meso* positions (*m* and *m'*) are also assigned here.

mono-metallic complex Fe(Cl)-PD_2 and the corresponding heterobimetallic complex, CoFe(Cl)-PD_2, were synthesized under similar reaction condition employed for synthesis of Fe(Cl)-PD_1 and CoFe(Cl)-PD_1, respectively. The resulting heterobimetallic complex, CoFe(Cl)-PD_2, was characterized by UV-Vis-NIR, ^{1}H NMR and ESI-MS. The UV-Vis spectrum of CoFe(Cl)-PD_2 in dichloromethane solution produces a sharp Soret band at 402 nm along with two Q bands at 498 and 663 nm (Fig. 4). Scheme 2 shows the synthetic outline of the homo and heterobimetallic complexes using ethene-bridged porphyrin dimer while the detailed synthetic procedures and spectral characterizations are given in the Experimental section.

Splitting of the Soret band into two well-resolved transitions has been the hallmark for the *anti* and *trans*-form which originates from the exciton coupling of $B_\perp$ and $B_{||}$ electronic transitions and associated with Kasha's exciton coupling theory[17]. The high-energy transition is associated with the transition dipole moment running through the 10,20-*meso* carbons ($B_\perp$) while the low energy transition is assigned to the transition dipole moment running through the 5,15-*meso* carbons ($B_{||}$). Such a split in the Soret band is clearly visible for homobimetallic complexes $Fe_2(Cl)_2$-PD_1 and $Fe_2(Cl)_2$-PD_2. In contrast, a sharp Soret band was observed in case of heterobimetallic porphyrin dimers CoFe(Cl)-PD_1 and CoFe(Cl)-PD_2 reported here.

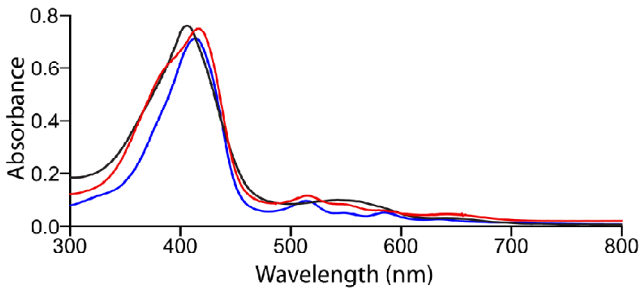

Fig. 2. UV-Visible spectra (at 295 K) in dichloromethane for PD_1 (blue), Fe(Cl)-PD_1 (red) and CoFe(Cl)-PD_1 (black).

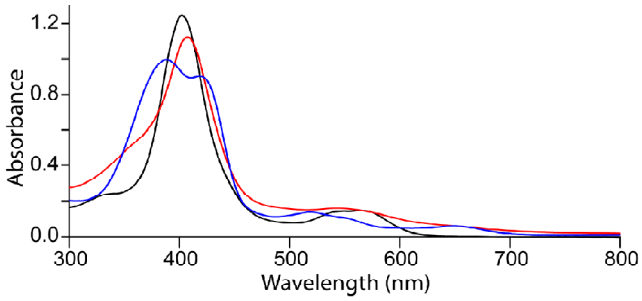

Fig. 3. UV-Visible spectra (at 295 K) in dichloromethane for $Fe_2(Cl)_2$-PD_1 (blue), Co_2-PD_1 (black) and CoFe(Cl)-PD_1 (red).

UV-Vis spectrum of heterobimetallic porphyrin dimer CoFe(Cl)-PD_1 is clearly distinguishable from its homobimetallic analogous, $Fe_2(Cl)_2$-PD_1 and Co_2-PD_1. The Soret band is red shifted in CoFe(Cl)-PD_1 (405 nm) with respect to its homometallic complex Co_2-PD_1. However, unlike the splitting pattern observed for the Soret band of $Fe_2(Cl)_2$-PD_1, a single peak appeared for heterobimetallic complex FeCo-PD_1. Also, in comparison to Co_2-PD_1 and $Fe_2(Cl)_2$-PD_1, the Q bands of CoFe(Cl)-PD_1 are broader and not distinguishable. The UV-Visible spectra for $Fe_2(Cl)_2$-PD_1, Co_2-PD_1 and CoFe(Cl)-PD_1 are compared in Fig. 3. UV-Vis spectrum of heterobimetallic porphyrin dimer CoFe(Cl)-PD_2 is also quite different as compared to its homobimetallic analogous, $Fe_2(Cl)_2$-PD_2 and Co_2-PD_2 (Fig. 4). While Co_2-PD_2 complex shows a sharp Soret band at 402 nm and Q bands at 401, 547 and 565 nm, splitting of the Soret band into two well-resolved bands at 391 and 412 nm has been clearly observed for $Fe_2(Cl)_2$-PD_2 along with Q bands at 517 and 645 nm in solution. In contrast, a broad Soret band is observed at 402 nm in case of heterobimetallic porphyrin dimer CoFe(Cl)-PD_2

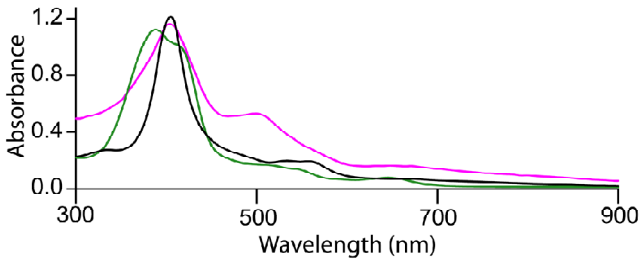

Fig. 4. UV-Visible spectra (at 295 K) in dichloromethane for $Fe_2(Cl)_2$-PD_2 (green), Co_2-PD_2 (black) and CoFe(Cl)-PD_2 (pink).

reported here. Fig. 4 displays UV-Visible spectra of $Fe_2(Cl)_2$-PD_2, Co_2-PD_2 and CoFe(Cl)-PD_2. Also, UV-Visible spectra of CoFe(Cl)-PD_1 and CoFe(Cl)-PD_2 are compared in Fig. 5 which clearly display the effect of the conjugation through an ethene-bridge in CoFe(Cl)-PD_2.

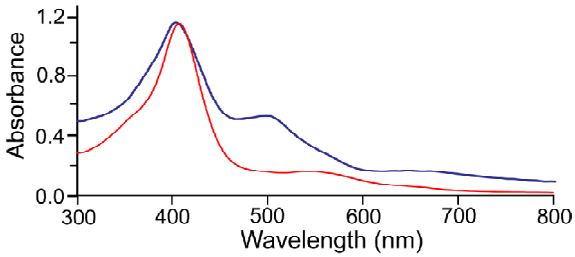

Fig. 5. UV-Visible spectra (at 295 K) in dichloromethane of CoFe(Cl)-PD_1 (red) and CoFe(Cl)-PD_2 (blue).

Formation of CoFe(Cl)-PD_1 is confirmed through the ESI-MS spectrum which reveals a peak at *m/z* = 1205.6007 assigned to $[CoFe(Cl)\text{-}PD_1\text{-}Cl]^+$ (Fig. 6). Also, the experimental isotopic distribution pattern matches exactly with the theoretical pattern (Fig. 6) which confirms the formation of the complex. The mass difference between two neighbouring peaks also confirms the monopositive state of the complex in the ESI(+) mode. The ESI-MS spectrum shows the intense molecular ion peak at *m/z* = 1239.5621 for $[CoFe(Cl)\text{-}PD_2 + H]^+$ (Fig. 7). In addition, a clear correlation is observed between the isotopic distribution pattern of the experimental mass with the theoretical one, thus confirming the formation of the complex (Fig. 7).

Crystallographic characterizations:

Dark brown crystals of $Fe_2(OCH_3)_2$-PD_1 and reddish brown crystals of CoFe(Cl)-PD_1 were obtained upon slow diffusion of methanol into a chloroform solution of the complexes at room temperature, from which appropriate crystals were chosen for X-ray structure determination. $Fe_2(OCH_3)_2$-PD_1 crystallizes in the triclinic system with *P*-1 space group, while CoFe(Cl)-PD_1 crystallizes in the monoclinic crystal system with *P*21/*c* space group. Perspective views of the $Fe_2(OCH_3)_2$-PD_1 and CoFe(Cl)-PD_1 are shown in Figs. 8 and 9, respectively. The molecules are in anti-conformation; the selected bond distances and angles of the molecules are

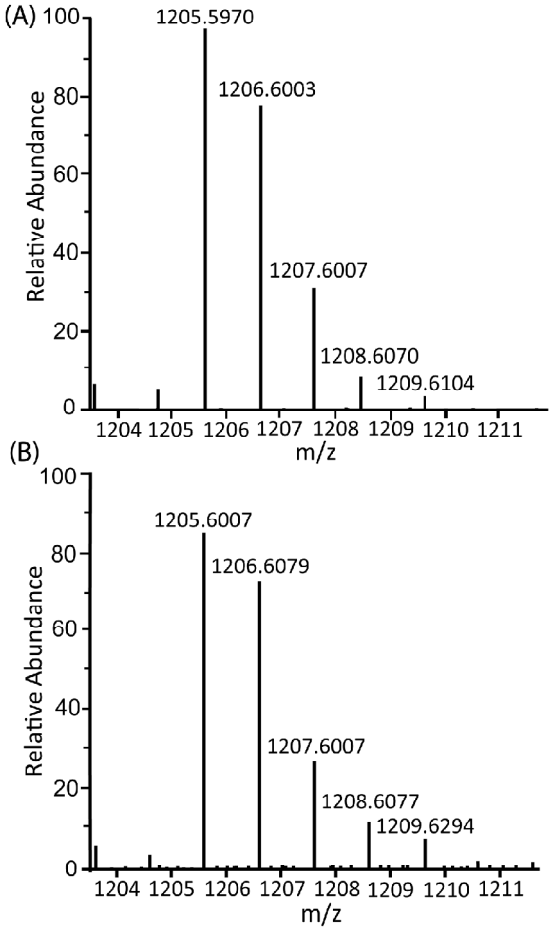

Fig. 6. Isotropic distribution of the (A) theoretical and (B) experimental MS (ESI) of $[CoFe(Cl)\text{-}PD_1 - Cl]^+$.

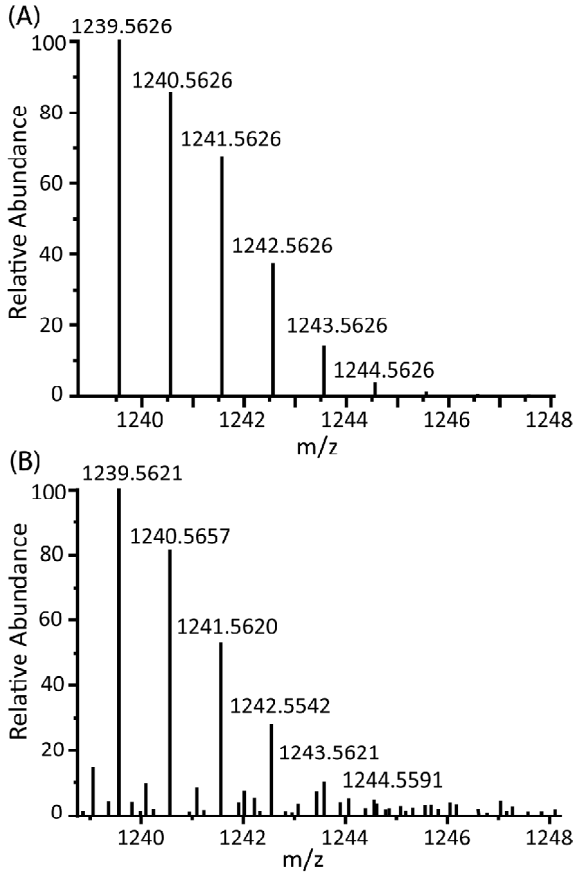

Fig. 7. Isotropic distribution of the (A) theoretical and (B) experimental MS (ESI) of $[CoFe(Cl)\text{-}PD_2 + H]^+$.

given in Table 1. Porphyrin rings are highly distorted while the distortion is less in the porphyrin that binds cobalt(II) ion. The Fe(III) centre has a distorted square-pyramidal geometry with a chlorine atom in the axial position and the equatorial sites being occupied by the N atom of the porphyrin ring. The Fe-Cl and the average Fe-N bond length in CoFe(Cl)-PD_1 are 2.214(5) and 2.045(7) Å, respectively, which are 'normal' for a high-spin iron(III) porphyrin with axial chloride ion[18–20]. The iron is displaced by 0.56 Å from the least-square plane of $C_{20}N_4$ porphyrinato core. Co(II) centre is four coordinated to the N atoms of the porphyrin ring in a square-planar geometry with an average Co-N bond length of 1.974(7) Å, which is similar to other four-coordinate Co(II) porphyrins reported in the literature.

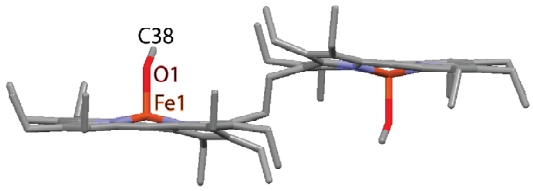

Fig. 8. Molecular structure (at 100 K) of $Fe_2(OCH_3)_2$-PD_1.

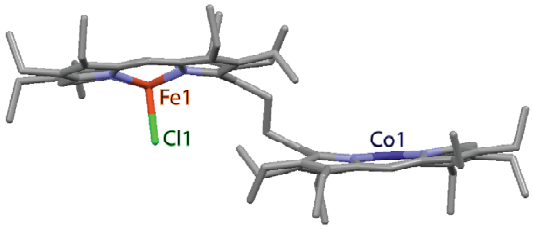

Fig. 9. Molecular structure (at 100 K) of CoFe(Cl)-PD_1.

Table 1. Selected distances (Å) and angles (°) for the Fe(III) complexes

	CoFe(Cl)-PD_1	$Fe_2(OCH_3)_2$-PD_1
Fe1-N1	2.075(7)	2.064(3)
Fe1-N2	2.029(7)	2.075(3)
Fe1-N3	2.025(7)	2.060(3)
Fe1-N4	2.052(7)	2.064(3)
Fe1-C11/O1	2.214(5)	2.005(4)
Co1-N1	1.973(7)	–
Co1-N2	1.980(7)	–
Co1-N3	1.974(7)	–
Co1-N4	1.972(7)	–
N1-Fe1-N2	86.9(3)	89.37(13)
N1-Fe1-N4	84.9(3)	87.45(13)
N2-Fe1-N4	150.9(2)	162.54(14)
N3-Fe1-N1	148.4(2)	160.12(14)
N3-Fe1-N2	85.4(3)	87.15(13)
N3-Fe1-N4	87.2(3)	90.02(13)
N1-Fe1-O1/C11	109.2(3)	101.20(14)
N2-Fe1-O1/C11	103.2(3)	99.04(14)
N3-Fe1-O1/C11	102.4(3)	98.68(14)
N4-Fe1-O1/C11	105.8(3)	98.41(14)

^{1}H NMR:

^{1}H NMR is a very powerful tool to analyse the molecular structure and properties in solution. This is more so for the molecules that are paramagnetic in nature. Interestingly, both iron(III) and Co(II) centers are paramagnetic in the heterobimetallic complexes reported here and it would be interesting to investigate how two paramagnetic centers influence each other while connected through a non-conjugated (ethane) and conjugated (ethene) bridge. ^{1}H NMR spectral investigations are highly informative and easier to visualize due to wide spectral range that varies from large positive to a large negative spectral regions. Indeed, ^{1}H NMR spectroscopy serves as a spectral probe for identifying different spin states of iron porphyrin in solution.

^{1}H NMR signals of the heterobimetallic complexes are very broad while the signals are spread from large upfield to large downfield regions due to the presence of two paramagnetic metal centers in the molecule. Porphyrin ring protons display characteristic signals in the ^{1}H NMR spectrum which depend on the electronic state of the paramagnetic centers. For example, the spectrum of $Fe_2(Cl)_2$-PD_2 (Fig. 10) displays the presence of eight methylene proton signals between 36.4 to 46.7 ppm, two upfield shifted *meso* signals in 2:1 intensity ratio at –68.2 and –52.0 ppm and a highly downfield shifted bridging signal at 112.2 ppm[12d]. The resonances for methyl protons are observed in the diamagnetic window since they are far off from the metal center and thus less influenced by the paramagnetic effect of metal unpaired spins. Similar is the situation for $Fe_2(Cl)_2$-PD_1 (Fig. 11) also[12c].

It would be useful now to discuss the ^{1}H NMR spectra for dicobalt(II) porphyrin dimers. By exploiting the influence of paramagnetic cobalt(II) ion, overall geometry of the molecule can also be clearly identified since two paramagnetic Co(II)OEP unit would be influenced by each other's presence in space also. For a four-coordinated square-planar Co(II)OEP, it is expected that there should be two *meso* proton signals in 1:2 intensity ratio, four methylene resonances and two methyl resonances. For Co_2-PD_1 four methylene proton signals are observed at 9.8, 9.6, 9.4 and 8.8 ppm, two *meso* signals at 28.8 and 25.6 ppm in 1:2 ratios while the bridging methylene signal arises at 12.3 ppm (Fig. 11)[12b]. This suggests that two Co(II)OEP units in the complex are equivalent in solution while the positioning of the methylene and *meso* signals provide unequivocal evidence for low-spin nature of the complex. The large separation between the two *meso* signals are also indicative of cofacial nature of the rings for its *syn* conformation[12b]. Co_2-PD_2 also demonstrates similar but clearly distinct paramagnetic shifts of the proton signals (Fig. 10). Eight methylene proton resonances and two well-separated *meso* signals in a 1:2 intensity ratio are due to cofacial arrangement of two porphyrin macro-cycles as expected for a *cis* isomer[12a].

The ^{1}H NMR spectra of polycrystalline samples of CoFe(Cl)-PD_1 and CoFe(Cl)-PD_2 are compared in Fig. 12. All the signals are well-resolved and are assigned; signals from both iron and cobalt centers are clearly visible. Eight methylene proton signals of the porphyrin ring coordinated to the Fe(III) center are observed between 34.7 to 44.0 ppm and between 34.8 to 43.6 ppm for CoFe(Cl)-PD_1 and CoFe(Cl)-PD_2, respectively. Two upfield shifted *meso* signals are in 2:1 intensity ratio and perceived at –55.5 and

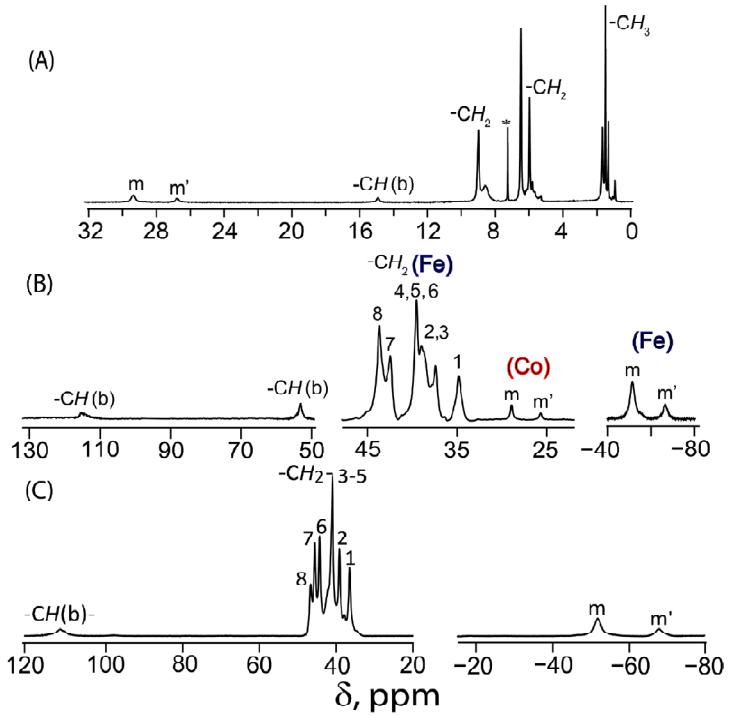

Fig. 10. ^{1}H NMR spectra (in $CDCl_3$ at 295 K) of (A) Co_2-PD_2, (B) CoFe(Cl)-PD_2 and (C) $Fe_2(Cl)_2$-PD_2. Here, -C*H*(b) marks the bridging protons and *m*, *m′* represents the *meso* proton (Scheme 2) signals.

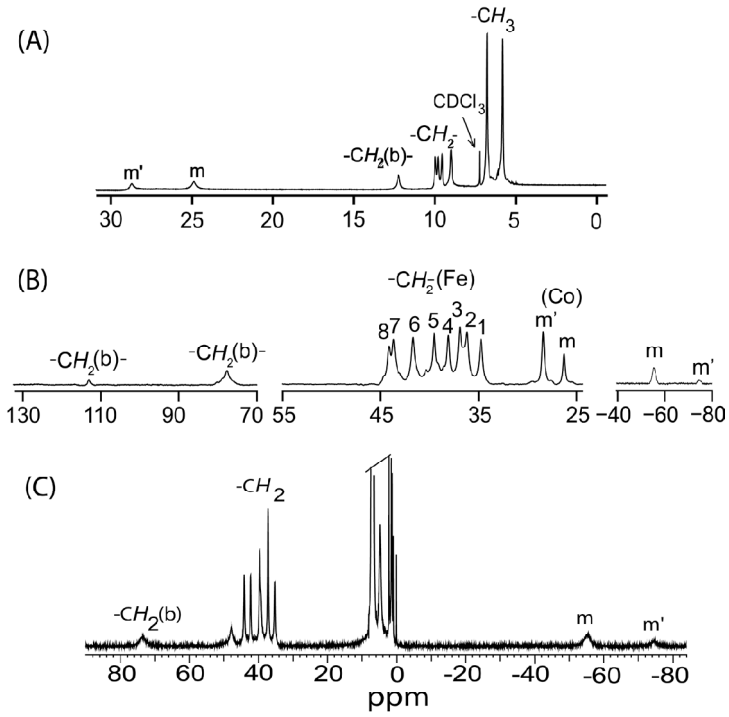

Fig. 11. ^{1}H NMR spectra (in $CDCl_3$ at 295 K) of (A) Co_2-PD_1, (B) CoFe(Cl)-PD_1 and (C) $Fe_2(Cl)_2$-PD_1. Here, -CH_2(b) marks the bridging protons and *m*, *m′* represents the *meso* proton (Scheme 1) signals.

–74.6 ppm in CoFe(Cl)-PD_1 and at –51.7 and –66.8 ppm in CoFe(Cl)-PD_2, for the porphyrin ring coordinated to the Fe(III) centre. This is similar to the chemical shift values observed for methylene and *meso* protons for $Fe_2(Cl)_2$-PD_1 and $Fe_2(Cl)_2$-PD_2 (Figs. 10 and 11)[12c,d]. Two downfield shifted *meso* signals are observed in 2:1 intensity ratio for the porphyrin ring coordinated to the Co(II) centre at 26.2 and 28.3 ppm in CoFe(Cl)-PD_1 and at 25.6 and 28.8 ppm in CoFe(Cl)-PD_2 (Fig. 12). Two bridging CH_2 proton signals are observed at 77.6 and 113.0 ppm in CoFe(Cl)-PD_1 and two bridging C*H* proton signals are observed at 53.2 and 114.7 ppm in CoFe(Cl)-PD_2 (Fig. 12). The bridging CH_2 proton signals are shifted far downfield in the heterobimetallic complex as compared to the respective CH_2 proton signals of the analogous homobimetallic complexes $Fe_2(Cl)_2$-PD_1 and Co_2-PD_1. The appearance of two bridging CH_2 and C*H* signals in CoFe(Cl)-PD_1 and CoFe(Cl)-PD_2, respectively, indicates two different metalloporphyrin centres connected through the ethane or ethene bridge in CoFe(Cl)-PD_1 and CoFe(Cl)-PD_2 which makes the bridging protons inequivalent in these complexes. This is unlike their homobimetallic analogues, wherein only a single proton signal is observed for the bridging CH_2 and C*H* proton (Figs. 10 and 11). The chemical shifts of the *meso* and methylene proton resonances are highly susceptible to the iron spin states[20,21] and from the spectral pattern in CoFe(Cl)-PD_1 and CoFe(Cl)-PD_2 it is evident that the iron(III) centre is found in high-spin state in solution.

Here, -C*H*(b) and CH_2(b) mark the bridging protons and *m*, *m′* represent the *meso* proton (Schemes 1 and 2) signals.

^{1}H NMR spectra of the heterobimetallic complexes are very different as compared to their homobimetallic analogs (Figs. 10 and 11). Both iron(III) and Co(II) centers are paramagnetic and their influences on each other, either through the bond or through the space, are clearly visible here. Instead of a lone signal for the bridzing protons in the homobimetallic complex, two resonances are observed in the heterobimetallic complexes reported here. However, the seperation between two such bridzing proton signals is much larger in case of ethene-bridged complex CoFe(Cl)-PD_2. The notable spectral features in the heterobimetallic complexes reported here are: large downfield shift of the *meso* and bridging protons adjacent to the Co(II) porphyrin centre and upfield shift of the CH_2 protons of the porphyrin ring coordinated to the Fe(III) centre. Also, complete reverse ordering of the *meso* proton (*m* and *m′*) signals has been observed for the porphyrin ring coordinated to the Co(II) centre in the heterobimetallic complexes. Moreover, large spectral changes are observed on going from ethane to ethene-bridged heterobimetallic complex. For example, separation between *m* and *m′ meso* proton signals has decreased significantly in the porphyrin ring coordinated to the Co(II) centre while complete reversal of their ordering are observed for the porphyrin ring coordinated to the Fe(III) ion for the ethene-

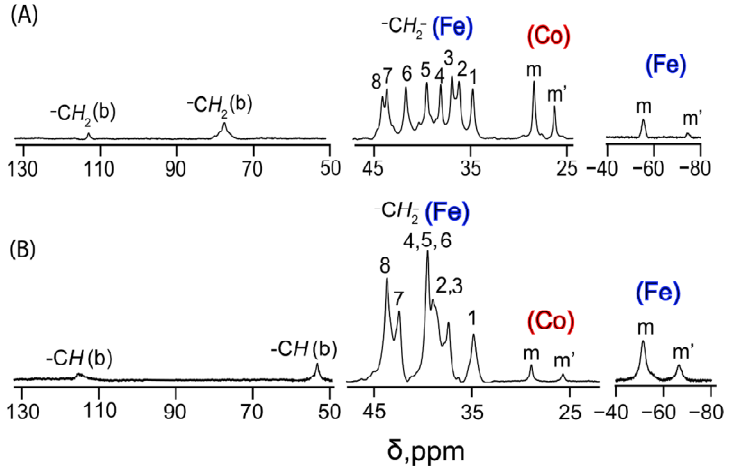

Fig. 12. ^{1}H NMR spectra (in $CDCl_3$ at 295 K) of (A) CoFe(Cl)-PD_1 and (B) CoFe(Cl)-PD_2.

bridged complex CoFe(Cl)-PD_2 in which electronic communication through the bridge is indeed possible.

The Curie plot (chemical shift versus 1/T) of the proton signals for CoFe(Cl)-PD_1 and CoFe(Cl)-PD_2 are shown in Figs. 13 and 14, respectively. The linear relationship of each signal indicates no change in the conformation of the complexes in solution. Moreover, the straight lines of the proton signals of CoFe(Cl)-PD_1 and CoFe(Cl)-PD_2 as per Curie law suggests the presence of single spin states of iron and cobalt centers across the temperature range[20,21].

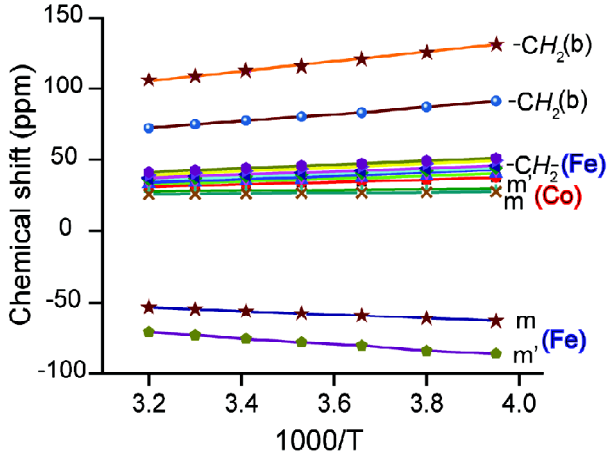

Fig. 13. Curie plot (δ vs 1000/T) of the proton signals of CoFe(Cl)-PD_1.

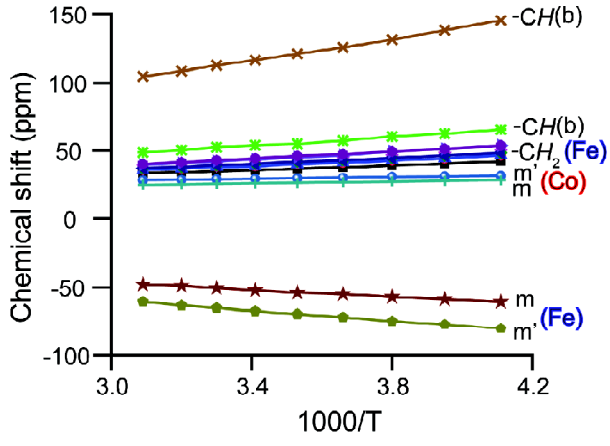

Fig. 14. Curie plot (δ vs 1000/T) of the proton signals of CoFe(Cl)-PD_2.

Magnetic measurements:

The magnetic susceptibility of CoFe(Cl)-PD_1 has been measured using an applied magnetic field of 0.1 T between 5 to 300 K and the data was fitted (Fig. 15) using the software PHI[22]. The parameters that are obtained from the fit are: J = –0.32 cm^{-1}, D = 7.0 cm^{-1}, TIP (temperature independent paramagnetism) = 5.2×10^{-5} cm^3 mol^{-1} and paramagnetic impurities = 2.4×10^{-3} cm^3 mol^{-1}. As can be seen, the coupling between Fe(III) and Co(II) unpaired spins is very small and antiferromagnetic in nature which is indeed.

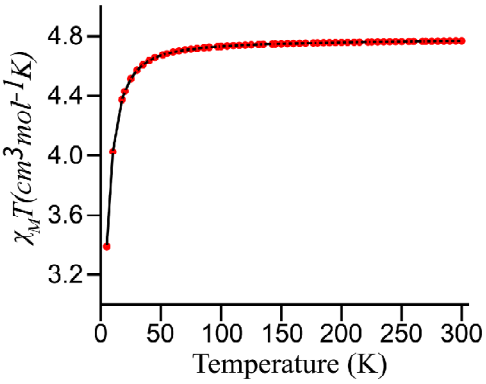

Fig. 15. X_MT versus T plot for CoFe(Cl)-PD_1. The solid line is the best fit using the values given in the text.

Summary

We have reported here the synthesis, structure and spectroscopic properties of Co(II)-Fe(III) heterobimetallic ethane and ethene-bridged porphyrin dimer and investigated spin coupling between two paramagnetic metal centers. X-Ray structures of one homobimetallic and one heterobimetallic complexes are reported here. UV-Vis spectrum of heterobimetallic complex is clearly distinguishable from its homobimetallic analogous, a split in the Soret band is clearly visible for homobimetallic complexes while a sharp Soret band was observed for heterobimetallic complexes. ^{1}H NMR spectra of the heterobimetallic complexes are different as compared to their homobimetallic analogs. Both Fe(III) and Co(II) centers are paramagnetic and their influences on each other, either through the bond or through the space, are clearly visible in the ^{1}H NMR spectra.

The Curie plot (chemical shift versus 1/T) of the proton signals for CoFe(Cl)-PD_1 and CoFe(Cl)-PD_2 display linear relationship of each signal indicating no change in the conformation of the complexes or spin state of the metal centers in solution. Variable temperature magnetic study demonstrates that the coupling between Fe(III) and Co(II) unpaired spins in CoFe(Cl)-PD_1 is very small and antiferromagnetic in nature which is indeed expected since both the rings are connected through an ethane-bridge and thus, through bond interaction is not possible.

Experimental section

Materials: 1,2-Bis(*meso*-octaethylporphyrinyl)ethane (PD_1) and 1,2-bis(*meso*-octaethylporphyrinyl)ethene (PD_2) was synthesized by modifying the literature method[14,16]. Reagents and solvents were purchased from commercial sources and were purified by standard procedures before use.

Synthesis of complex CoFe(Cl)-PD_1: 60 mg of PD_1 was dissolved in degassed $CHCl_3$ under N_2 atmosphere, and 1.2 equivalent of $FeCl_2$ (150 mg, 1.2 mmol) was added to it. The reaction mixture was refluxed under N_2 atmosphere for 1 h. After cooling to room temperature, the mixture was washed with 10% HCl solution. The organic layer was then separated and dried over anhydrous Na_2SO_4 and evaporated to complete dryness. The solid, thus obtained, was purified by column chromatography using a silica gel column. The major fraction (Fe(Cl)-PD_1) (see Scheme 1) eluted with chloroform was collected and then dried under vacuum. To the $CHCl_3$ solution of the monometallated porphyrin dimer, Fe(Cl)-PD_1, was added a methanolic solution of $Co(OAc)_2.4H_2O$ (1.2 equivalent) and the resulting mixture was refluxed under N_2 atmosphere for 1 hour. The organic layer was separated, dried over anhydrous Na_2SO_4 and evaporated to complete dryness. The solid thus obtained, was purified by column chromatography using neutral alumina. The major fraction (CoFe(Cl)-PD_1) eluted with 2% MeOH:$CHCl_3$ was collected and dried under vacuum. The resulting solid was then dissolved in a minimum volume of $CHCl_3$, filtered to remove any solid residue present and then carefully layered with CH_3OH. Upon slow evaporation at room temperature, red crystals of CoFe(Cl)-PD_1 were obtained, which were then isolated by filtration, washed with n-hexane, and dried under vacuum. Yield: 44 mg (39%). UV-Vis (dichloromethane) [λ_{max}, nm (μ, M^{-1} cm^{-1})]: 405 (7.5×10^4), 554 (1.0×10^4), 655 (5.3×10^3). ESI-MS: *m/z* 1205.6007 for [CoFe(Cl)-PD_1 – Cl^-]$^+$. ^{1}H NMR ($CDCl_3$, 295 K): *meso-H*: –74.6, –55.5, 26.2, 28.3; C*H*$_2$: 34.7, 36.0, 36.9, 38.0, 39.4, 41.6, 43.6, 44.0; C*H*$_2$(b): 113.0, 77.6 ppm.

Synthesis of CoFe(Cl)-PD_2: 60 mg of PD_2 was dissolved in degassed $CHCl_3$ under N_2 atmosphere, and 1.2 equivalent of $FeCl_2$ (150 mg, 1.2 mmol) was added to it. The reaction mixture was refluxed under N_2 atmosphere for 1 hour. After cooling to room temperature, the mixture was washed with 10% HCl solution. The organic layer was then separated and dried over anhydrous Na_2SO_4 and evaporated to complete dryness. The solid, thus obtained, was purified by column chromatography using a silica gel column. The major fraction (Fe(Cl)-PD_2) eluted with chloroform was collected and then dried under vacuum. To the $CHCl_3$ solution of the monometallated porphyrin dimer, Fe(Cl)-PD_2, was added a methanolic solution of 1.2 equivalent of $Co(OAc)_2.4H_2O$ and the resulting mixture was refluxed under N_2 atmosphere for 1 hour. The reddish-brown solution was then separated and dried over anhydrous Na_2SO_4 and evaporated to complete dryness. The solid thus obtained, was purified by column chromatography using neutral alumina. The first fraction (CoFe(Cl)-PD_2) eluted with chloroform was collected and dried under vacuum. Yield: 30 mg (27%). UV-Vis (dichloromethane) [λ_{max}, nm (μ, M^{-1} cm^{-1})]: 402 (1.5×10^4), 498 (6.8×10^3), 663 (2.1×10^3). ESI-MS: *m/z* = 1239.5621 for [CoFe(Cl)-PD_2 + H]$^+$. ^{1}H NMR ($CDCl_3$, 295 K): *meso-H*: –66.8, –51.7, 28.8, 25.6; C*H*$_2$: 34.8, 37.3, 39.5, 42.5, 43.6; C*H*(b): 114.7, 53.2 ppm.

Instrumentation: UV-Vis spectra were recorded on a Perkin-Elmer UV/Vis spectrometer. The ESI mass spectra were recorded with a Waters Micromass Quattro Micro triple quadrupole mass spectrometer. ^{1}H NMR spectra were recorded on a JEOL 500 MHz instrument. The spectra for paramagnetic molecules were recorded over a 100-kHz bandwidth with 64 K data points and a 5-ms 90° pulse. The residual ^{1}H resonances of the solvents were used as a secondary reference. Magnetic susceptibility data were collected using a Quantum Design MPMS SQUID magnetometer over the temperature range 5 to 300 K. The magnetic data were fitted using the software PHI[22]. One set of data were collected over the temperature range of 5 to 300 K, by using applied magnetic fields of 0.1 T.

X-Ray structure solution and refinement: Single-crystal X-ray data were collected at 100 K on a Bruker SMART APEX

CCD diffractometer equipped with CRYO Industries low temperature apparatus and intensity data were collected using graphite-monochromated Mo Kα radiation (λ = 0.71073 Å). The data integration and reduction were processed with SAINT software[23]. An absorption correction was applied[24]. The structure was solved by the direct method using SHELXS-97 and was refined on F2 by full-matrix least-squares technique using the SHELXL-2018 program package[25]. Non-hydrogen atoms were refined anisotropically. In the refinement, hydrogen was treated as riding atoms using SHELXL default parameters. Crystallographic data and data collection parameters are given in Table 2. CCDC 2048471 and 2048472 contains the supplementary crystallographic data of CoFe(Cl)-PD_1, and $Fe_2(OCH_3)_2$-PD_1, respectively, for this paper. These data can be obtained free of charge from The Cambridge Crystallographic Data Centre via www.ccdc.cam.ac.uk/data_request/cif.

Table 2. Crystallographic data and data collection parameters

	CoFe(Cl)-PD_1	$Fe_2(OCH_3)_2$-PD_1
Formula	$C_{74}H_{90}N_8ClCoFe$	$C_{76}H_{96}Fe_2N_8O_2$
T (K)	100(2)	100(2)
Formula weight	1241.76	1265.30
Crystal system	Monoclinic	Triclinic
Space group	*P*21/*c*	*P*-1
a (Å)	14.663(4)	10.6288(6)
b (Å)	17.422(5)	13.6421(7)
c (Å)	14.928(4)	14.0528(8)
α (°)	90	66.526(2)°
β (°)	93.254(6)°	68.981(2)°
γ (°)	90	82.744(2)°
V (Å^3)	3807.3(18)	1744.32(17)
Z	2	1
d_{calcd} (g.cm^{-3})	1.083	1.205
μ (mm^{-1})	0.485	0.466
F (000)	1320	676
No. of unique data	8664	6478
No. of parameters refined	513	406
GOF on F^2	1.039	1.092
R_1[a] [I > 2σ(I)]	0.0986	0.0711
R_1[a] (all data)	0.1721	0.0919
wR_2[b] (all data)	0.2730	0.1805
Largest diff. peak and hole	0.640 and –0.652 e.Å^{-3}	0.736 and –0.513 e.Å^{-3}

[a] $R_1 = \Sigma \,||F_o| - |F_c|| / \Sigma |F_o|$

[b] $wR_2 = [\,\Sigma[\,w(F_o^2 - F_c^2)^2]/\Sigma\,[w(F_o^2)^2]\,]^{1/2}$

Acknowledgements

We are thankful to Science and Engineering Research Board (SERB), India for financial support. SPR thanks SERB for Science and Technology Award for Research (SERB-STAR) to him. We thank Professor Raymond John Butcher for some help in solving one of the structure.

References

1. (a) J. Liu, S. Chakraborty, P. Hosseinzadeh, Y. Yu, S. Tian, I. Petrik, A. Bhagi and Y. Lu, *Chem. Rev*., 2014, **114**, 4366; (b) C. M. Paquete and R. O. Louro, *Acc. Chem. Res*., 2014, **47**, 56; (c) B. M. Fonseca, C. M. Paquete, C. A. Salgueiro and R. O. Louro, *FEBS Lett*., 2012, **586**, 504; (d) C. M. Soares and A. M. Baptista, *FEBS Lett*., 2012, **586**, 510; (e) J. A. Mayfield, C. A. Dehner and J. L. DuBois, *Curr. Opin. Chem. Biol*., 2011, **15**, 260.
2. (a) L. M. R. Jensen, R. Sanishvili, V. L. Davidson and C. M. Wilmot, *Science*, 2010, **327**, 1392; (b) V. L. Davidson and C. M. Wilmot, in: "Handbook of Porphyrin Science", eds. K. M. Kadish, K. M. Smith and R. Guilard, World Scientific Publishing, Singapore., 2016, Vol. 44, p 1; (c) M. Khademian and J. A. Imlay, *Proc. Natl. Acad. Sci. USA*, 2017, **114**, E6922; (d) J. Geng, K. Dornevil, I. Davis and A. Liu, *Proc. Natl. Acad. Sci. USA*, 2013, **110**, 9639.
3. (a) K. Rizzolo, S. E. Cohen, A. C. Weitz, M. M. L. Muñoz, M. P. Hendrich, C. L. Drennan and S. J. Elliott, *Nat Commun.*, 2019, **10**, 1101; (b) G. S. Pulcu, K. E. Frato, R. Gupta, H.-R. Hsu, G. A. Levine, M. P. Hendrich and S. J. Elliott, *Biochemistry,* 2012, **51**, 974; (c) J. Seidel, M. Hoffmann, K. E. Ellis, A. Seidel, T. Spatzal, S. Gerhardt, S. J. Elliott and O. Einsle, *Biochemistry,* 2012, **51**, 2747.
4. (a) A. Dhamija, P. Mondal, B. Saha and S. P. Rath, *Dalton Trans.*, 2020, **49**, 10679; (b) P. Mondal and S. P. Rath, *Coord. Chem. Rev.*, 2020, **405**, 213117; (c) D. Lai, F. S. T. Khan and S. P. Rath, *Dalton Trans.*, 2018, **47**, 14388; (d) T. Guchhait, S. Sasmal, F. S. T. Khan and S. P. Rath, *Coord. Chem. Rev.*, 2017, **337**, 112; (e) F. S. T. Khan, T. Guchhait, S. Sasmal and S. P. Rath, *Dalton Trans.*, 2017, **46**, 1012; (f) D. Sil and S. P. Rath, *Dalton Trans.*, 2015, **44**, 16195; (g) F. S. T. Khan, A. K. Pandey and S. P. Rath, *J. Chem. Sci.*, 2018, **130**, 85.
5. (a) P. Lang and M. Schwalbe, *Chem.-Eur. J.*, 2017, **23**, 17398; (b) V. Valderrey, G. Aragay and P. Ballester, *Coord. Chem. Rev*., 2014, **258**, 137; (c) J. Rosenthal and D. G. Nocera, *Acc. Chem. Res*., 2007, **40**, 543; (d) P. D. Harvey, C. Stern, C. P. Gros and R. Guilard, *Coord. Chem. Rev.*, 2007, **251**, 401.
6. (a) G. de la Torre, G. Bottari, M. Sekita, A. Hausmann, D. M. Guldi and T. Torres, *Chem. Soc. Rev.*, 2013, **42**, 8049; (b) D. Wrobel and A. Graja, *Coord. Chem. Rev*., 2011, **255**, 2555; (c) J. Rosenthal, J. Bachman, J. L. Dempsey, A. J. Esswein, T. G. Gray, J. M. Hodgkiss, D. R. Manke, T. D. Luckett, B. J. Pistorio, A. S. Veige and D. G. Nocera, *Coord. Chem. Rev*., 2005, **249**, 1316.

7. (a) T. Tanaka and A. Osuka, *Chem. Soc. Rev.,* 2015, **44**, 943; (b) Y. Terazono, G. Kodis, M. Chachisvilis, B. R. Cherry, M. Fournier, A. Moore, T. A. Moore and D. Gust, *J. Am. Chem. Soc.*, 2015, **137**, 245; (c) J. Yang, M.-C. Yoon, H. Yoo, P. Kim and D. Kim, *Chem. Soc. Rev.*, 2012, **41**, 4808.
8. (a) F. S. T. Khan, S. Banerjee, D. Kumar and S. P. Rath, *Inorg. Chem.*, 2018, **57**, 11498; (b) F. S. T. Khan, A. Kumar, D. Lai and S. P. Rath, *Inorg. Chim. Acta*, 2019, **484**, 503; (c) F. S. T. Khan, A. K. Pandey and S. P. Rath, *Chem.-Eur. J.*, 2016, **22**, 16124; (d) D. Sil, F. S. T. Khan and S. P. Rath, *Chem.-Eur. J.*, 2016, **22**, 14585; (e) D. Sil, A. Kumar and S. P. Rath, *Chem.-Eur. J.*, 2016, **22**, 11214; (f) D. Sil, S. Bhowmik, F. S. T. Khan and S. P. Rath, *Inorg. Chem.*, 2016, **55**, 3239; (g) M. A. Sainna, D. Sil, D. Sahoo, B. Martin, S. P. Rath, P. Comba and S. P. de Visser, *Inorg. Chem.*, 2015, **54**, 1919; (h) D. Sil, F. S. T. Khan and S. P. Rath, *Inorg. Chem.*, 2014, **53**, 11925; (i) S. Bhowmik, S. K. Ghosh, S. Layek, H. C. Verma and S. P. Rath, *Chem.-Eur. J.*, 2012, **18**, 13025; (j) S. K. Ghosh and S. P. Rath, *J. Am. Chem. Soc.*, 2010, **132**, 17983; (k) S. K. Ghosh, R. Patra and S. P. Rath, *Inorg. Chem.,* 2008, **47**, 10196.
9. (a) F. S. T. Khan, S. J. Shah, S. Bhowmik, F. G. C. Reinhard, M. A. Sainna, S. P. de Visser and S. P. Rath, *Dalton Trans.*, 2019, **19**, 6353; (b) A. K. Pandey, S. Sanfui, F. S. T. Khan and S. P. Rath, *J. Organomet. Chem.*, 2019, **894**, 28; (c) S. Bhowmik, S. Dey, D. Sahoo and S. P. Rath, *Chem.-Eur. J.*, 2013, **19**, 13732; (d) S. Bhowmik, D. Sil, R. Patra and S. P. Rath, *J. Chem. Sci.,* 2011, **123**, 827; (e) S. Bhowmik, S. K. Ghosh and S. P. Rath, *Chem. Commun.*, 2011, **47**, 4790.
10. (a) A. K. Singh, F. S. T. Khan and S. P. Rath, *Angew. Chem. Int. Ed.*, 2017, **56**, 8849; (b) A. K. Singh, M. Usman, G. Sciortino, E. Garribba and S. P. Rath, *Chem.-Eur. J.*, 2019, **25**, 10098; (c) A. K. Singh and S. P. Rath, *Chem.-Eur. J.*, 2020, **26**, 14405.
11. (a) T. Guchhait, S. Sarkar, Y. A. Pandit and S. P. Rath, *Chem.-Eur. J.*, 2017, **23**, 10270; (b) Y. A. Pandit, S. Sanfui and S. P. Rath, *Chem.-Eur. J.*, 2017, **23**, 13415.
12. (a) S. Dey, D. Sil and S. P. Rath, *Angew. Chem. Int. Ed.*, 2016, **55**, 996; (b) S. Dey and S. P. Rath, *Dalton Trans.*, 2014, **43**, 2301; (c) S. K. Ghosh, R. Patra and S. P. Rath, *Inorg. Chem.*, 2010, **49**, 3449; (d) S. K. Ghosh, R. Patra and S. P. Rath, *Inorg. Chim. Acta*, 2010, **363**, 2791.
13. (a) A. Kumar, S. Sanfui, G. Sciortino, J.-D. Maréchal, E. Garribba and S. P. Rath, *Chem.-Eur. J.*, 2020, **26**, 7869; (b) A. Kumar, D. Sil, M. Usman and S. P. Rath, *Chem. Commun.*, 2019, **55**, 1588; (c) A. K. Pandey, M. Usman and S. P. Rath, *Chem. Commun.*, 2019, **55**, 7926; (d) A. Kumar, S. Banerjee, S. Sarkar and S. P. Rath, *Dalton Trans.*, 2019, **48**, 10089; (e) Y. A. Pandit, S. J. Shah and S. P. Rath, Z. *Anorg. Allg. Chem.*, 2018, **644**, 856; (f) D. Sil, S. Dey, A. Kumar, S. Bhowmik and S. P. Rath, *Chem. Sci.*, 2016, **7**, 1212; (g) S. Dey, D. Sil, Y. A. Pandit and S. P. Rath, *Inorg. Chem.*, 2016, **55**, 3229.
14. (a) T. E. Clement, D. J. Nurco and K. M. Smith, *Inorg. Chem.*, 1998, **37**, 1150; (b) M. O. Senge, M. Graca, H. Vicente, K. R. Gerzevske, T. M. Forsyth and K. M. Smith, *Inorg. Chem.*, 1994, **33**, 5625.
15. (a) J. P. Collman, P. S. Wagenknecht and J. E. Hutchison, *Angew. Chem. Int. Ed.*, 1994, **33**, 1537; (b) M. S. Asano, M. Shibuki and T. Otsuka, *Chem. Lett.*, 2016, **45**, 1114; (c) V. V. Borovkov, J. M. Lintuluoto and Y. Inoue, *Helv. Chim. Acta*, 1999, **82**, 919; (d) S. Brandes, A. Tabard, N. Bouhmaida, C. Lecomte, P. Richard, S. Brandes, J. M. Latoulc and R. Guilard, *J. Am. Chem. Soc.*, 1994, **116**, 10202; (e) M. A. Lopez, A. Tabard, P. Richard, C. Lecomte, S. Brandes, J. E. Hutchison, J. P. Collman and R. Guilard, *J. Am. Chem. Soc.*, 1992, **114**, 9877.
16. (a) L. J. Sessler, A. Mozaffari and M. R. Johnson, *Org. Synth.*, 1992, **70**, 68; (b) D. Arnold, A. W. Johnson and M. Winter, *J. Chem. Soc., Perkin Trans.*, 1977, **1**, 1643.
17. M. Kasha, H. R. Rawls and M. A. E. Bayoumi, *Pure Appl. Chem.*, 1965, **11**, 371.
18. (a) R. Weiss, A. Gold and J. Terner, *Chem. Rev.*, 2006, **106**, 2550; (b) M. Nakamura, *Coord. Chem. Rev.*, 2006, **250**, 2271; (c) Y. Ling and Y. Zhang, *J. Am. Chem. Soc.*, 2009, **131**, 6386.
19. (a) W. R. Scheidt, in: "The Porphyrin Handbook", eds. K. M. Kadish, K. M. Smith and R. Guilard, Academic Press, San Diego, 2000, Vol. 3, p. 49; (b) W. R. Scheidt and C. A. Reed, *Chem. Rev.*, 1981, **81**, 543.
20. (a) D. Sahoo, S. Roy, F. S. T. Khan, A. K. Singh and S. P. Rath, *Polyhedron,* 2019, **172**, 8; (b) D. Sahoo, M. G. Quesne, S. P. de Visser and S. P. Rath, *Angew. Chem. Int. Ed.*, 2015, **54**, 4796; (c) D. Sahoo and S. P. Rath, *Chem. Commun.*, 2015, **51**, 16790; (d) D. Sahoo, T. Guchhait and S. P. Rath, *Eur. J. Inorg. Chem.*, 2016, 3441; (e) D. Sahoo, A. K. Singh, and S. P. Rath, *Eur. J. Inorg. Chem.*, 2016, 3305; (f) R. Patra, D. Sahoo, S. Dey, D. Sil and S. P. Rath, *Inorg. Chem.*, 2012, **51**, 11294; (g) A. Chaudhary, R. Patra and S. P. Rath, *Indian J. Chem., Sect. A,* 2011, 432; (h) A. Chaudhary, R. Patra and S. P. Rath, *Eur. J. Inorg. Chem.,* 2010, 5211; (i) R. Patra, S. Bhowmik, S. K. Ghosh and S. P. Rath, *Dalton Trans.,* 2010, **39**, 5795; (j) R. Patra, S. Bhowmik, S. K. Ghosh and S. P. Rath, *Eur. J. Inorg. Chem.,* 2009, **5**, 654; (k) R. Patra and S. P. Rath, *Inorg. Chem. Commun.*, 2009, 515; (l) R. Patra, A. Chaudhury, S. K. Ghosh and S. P. Rath, *Inorg. Chem.*, 2008, **47**, 8324; (m) S. P. Ghosh, R. Patra and S. P. Rath, *Inorg. Chem.,* 2008, **47**, 9848.
21. (a) S. Kouno, A. Ikezaki, T. Ikeue and M. Nakamura, *J. Biol. Inorg. Chem.*, 2011, **105**, 718; (b) F. A. Walker, in: "Handbook of Porphyrin Science", eds. K. M. Kadish, K. M. Smith and R. Guilard, World Scientific, Singapore, 2010, Vol. 6, p. 1.
22. N. F. Chilton, R. P. Anderson, L. D. Turner, A. Soncini and K. S. Murray, *J. Comput. Chem.,* 2013, **34**, 1164.
23. SAINT+, 6.02 ed., Bruker AXS, Madison, WI, 1999.
24. G. M. Sheldrick, SADABS 2.0, 2000.
25. G. M. Sheldrick, SHELXL-2018: Program for Crystal Structure Refinement, University of Göttingen, Göttingen, Germany, 2018.